Unravelling the effect of alkali cations and halide anions on the de-hydrogenation properties of ammine zinc borohydrides

Parviz Hajiyev, Vasile Iosub, Michel Bardet, Stephanie Pouget, François Rieutord, Philippe Capron

Unravelling the effect of alkali cations and halide anions on the de-hydrogenation properties of ammine zinc borohydrides

Parviz HAJIYEV[a], Vasile IOSUB[a], Michel BARDET[b], Stephanie POUGET[b], François RIEUTORD[b], Philippe CAPRON[a]

[a] Univ. Grenoble Alpes, CEA, Liten, DTNM, 38000 Grenoble, France

[b] Univ. Grenoble Alpes, CEA, IRIG, 38000 Grenoble, France.

vasile.iosub@cea.fr

michel.bardet@cea.fr

stephanie.pouget@cea.fr

francois.rieutord@cea.fr

philippe.capron@cea.fr

Corresponding Author:

Email: parviz.hajiyev@cea.fr

Tel: +33 43 87 86 947

Postal address: 17 Avenue des Martyrs, 38000 Grenoble, France

Abstract
This work sheds light on the role of the alkali cations, halide anion substitution as well as borohydride anion vacancies on the de-hydrogenation properties of ammine zinc borohydrides. A new liquid ammonia-based synthesis approach employed in this study enabled direct solvothermal synthesis of several novel and previously reported ammine zinc borohydride compounds such as $A_xZn(BH_4)_{2+x}(NH_3)_2$ for x = 0; 1 and M = Li; Na; K. The experimental results are supported by first principle calculations and molecular dynamics techniques for the interpretation of inherently complex hydrogen release mechanisms. We demonstrate that the salt metathesis reaction heavily relied upon in literature for synthesis of these compounds can result in preferential halide anion substitution of certain borohydride sites in the structure which have significant consequences for hydrogen storage properties. Conclusions of this work is applicable not only to zinc system but to any ammine metal borohydride system.

Graphical Abstract

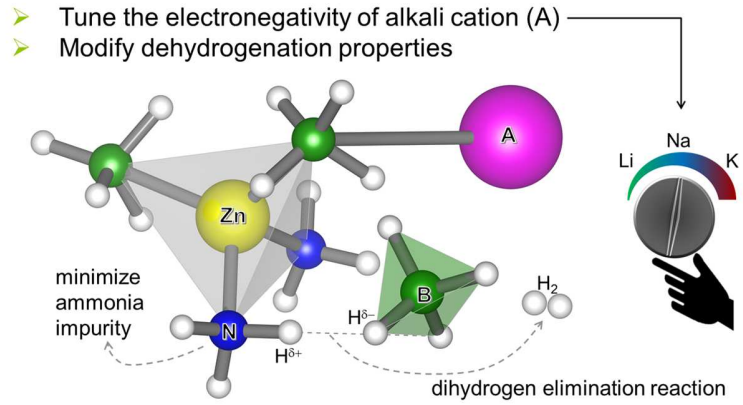

Keywords
Ammine metal borohydrides, ammonia, hydrogen

1. Introduction

Due to the intermittent nature of renewable energy sources, to facilitate their large scale adoption it is crucial to develop energy storage technologies. For mobile and short-term energy storage, the battery type electrochemical storage technologies have superiority. However, for long term (seasonal, annual) storage of energy - excluding compressed air and pumped hydro technologies which are limited by available geographical features - hydrogen storage remains the only scalable technological solution. The possibility for developing superior technologies to liquid and compressed hydrogen storage is still open thanks to recent advances in chemical storage approaches based on light molecules such as ammonia, liquid organic hydrogen carriers and metal borohydrides [1],[2]. Main advantages of chemical storage over physical storage are improved safety and storage capacity. However, the kinetics, cyclability, overall energetic efficiency and economic viability for the large-scale applications remain as some of the main challenges. The research in metal borohydrides and their ammoniates has been reignited during the last decade as potential chemical hydrogen storage materials [3]. With up to 15 wt% experimental hydrogen capacity with relatively high purity (> 97 mol%) the ammine metal borohydride (AMB) compounds such $Li_2Al(BH_4)_5(NH_3)_6$ and $Li_2Ti(BH_4)_5(NH_3)_5$ are among the best examples [4],[5]. Nevertheless, several drawbacks of these compounds still need to be resolved, the main one being the released ammonia impurity which is not well understood. The new liquid ammonia based synthesis technique enabled the synthesis of several ammine zinc borohydride (AZB) compounds. Hence, we chose AZB family as a testbed to unravel the role of alkali cations and various defects in these solid state hydrogen storage materials.

Zinc borohydride compounds

Makhaeva et al presented first bimetallic zinc borohydrides in 1974, reportedly the reaction of $ZnCl_2$ and $LiBH_4$ in 1:2 ratio in diethyl ether (Et_2O) solvent results in formation of $Li_yZnCl_{x+y}(BH_4)_{2-x}$ type equilibrium phase. Despite LiCl byproduct being almost insoluble in Et_2O, the equilibrium phase is obtained due to solubility of LiCl in the presence of $Zn(BH_4)_2$ as $LiZnCl(BH_4)_2$ species. Nevertheless, chloride-free $Li_2Zn(BH_4)_4{\cdot}3Et_2O$ solvate can be obtained by using $LiBH_4$ in excess (in 1:4 molar ratio) [6]. Unlike lithium borohydride, $NaBH_4$ is insoluble in Et_2O. Nonetheless, due to slight solubility of $ZnCl_2$ in ether, the reaction does take place in excess of $NaBH_4$ although much slowly, resulting in formation of bimetallic borohydride phase, $NaZn(BH_4)_3$. By contrast, formation of this phase is much faster in tetrahydrofuran (THF). $NaZn(BH_4)_3{\cdot}3Et_2O$ and $NaZn(BH_4)_3{\cdot}4THF$ type solvates can be extracted from these solutions. Both solvates under dynamic vacuum yields crystalline $NaZn(BH_4)_3$ [7]. KBH_4 is not soluble in both THF and Et_2O. Its reaction with $ZnCl_2$ in Et_2O even in 1:10 ratio does not yield $KZn(BH_4)_3$ phase; instead, the main product is $K_2Zn_3(BH_4)_8{\cdot}xEt_2O$ solvate [8].

In fact, synthesis of monometallic $Zn(BH_4)_2{\cdot}2Et_2O$ solvate phase requires specific precursors and reaction conditions. In 1951 Schlesinger et al first reported the formation of $Zn(BH_4)_2$ in Et_2O. This was achieved by allowing the suspension of ZnH_2 in diethyl ether to absorb the diborane gas. The elemental analysis showed the formation of $Zn(BH_4)_2$. They prepared ZnH_2 as a precipitate in ether through the reaction of dimethylzinc $Zn(CH_3)_2$ with lithium alanates $LiAlH_4$. White non-volatile ZnH_2 is reported to be stable in air, but gradually turned grey becoming pyrophoric in the matter of days [9]. Organozinc ZnR_2 (where R = CH_3 or C_2H_5) compounds react with diborane gas to form $Zn(BH_4)_2$. However, self-igniting pyrophoric nature of these precursors is a major safety drawback [10]. Although synthesis of pure zinc borohydride is possible with expensive organozinc precursors, needless to say that the rewards outweigh the risks.

Under dynamic vacuum, $Zn(BH_4)_2{\cdot}2Et_2O$ solvate easily turns into oily $Zn(BH_4)_2{\cdot}Et_2O$ which is stable up to 60°C. Nevertheless, removal of last ether adduct results in rapid decomposition of

pure $Zn(BH_4)_2$. Crystalline $Zn(BH_4)_2{\cdot}2THF$ solvate can be obtained at RT which melts at 67°C. Stronger Lewis bases such as pyridine, trimethylamine and ammonia can displace Et_2O or THF adducts in the solvate. By these approaches, the crystalline solvates of $Zn(BH_4)_2{\cdot}2Py$, $Zn(BH_4)_2{\cdot}2TMA$ and $Zn(BH_4)_2{\cdot}4NH_3$ were reportedly prepared [10]. No crystalline information was provided for these powders, the main characterization was performed using elemental analysis. Although, the behavior of $[BH_4]^-$ anion as pseudo-halide similar to the Cl^- anion in $Zn(NH_3)_2Cl_2$ is discussed, the solvate nevertheless identified as $Zn(BH_4)_2{\cdot}4NH_3$ [10]. More recently, Gu et al successfully synthesized $Zn(BH_4)_2{\cdot}2NH_3$ and resolved its crystal structure by synchrotron XRD analysis. The main phase together with LiCl byproduct is obtained by mechanochemical synthesis between $Zn(NH_3)_2Cl_2$ and $LiBH_4$ [11].

The mechanochemical synthesis through salt metathesis reaction of zinc chloride and alkali borohydrides results in formation of several bimetallic borohydrides such $LiZn_2(BH_4)_5$, $NaZn_2(BH_4)_5$, $NaZn(BH_4)_3$ [12], as well as mixtures of $KZn(BH_4)_3$ and $K_2Zn(BH_4)_xCl_{4-x}$ with $K_3Zn(BH_4)_xCl_{5-x}$ impurities [13]. All of these compounds are also contaminated with corresponding alkali halide or complex halide A_xZnCl_{2+x} byproducts. However, Xia et al reported THF assisted ball-milling of $ZnCl_2$:$NaBH_4$ in 1:3 ratio which results in precipitation of NaCl byproduct from the $NaZn(BH_4)_3{\cdot}nTHF$ solution. After NaCl filtration, subsequent treatment of this solution with ammonia atmosphere precipitated white $NaZn(BH_4)_3{\cdot}2NH_3$ powder in THF [7]. To the best of our ability we were not successful in desolvation of the $NaZn(BH_4)_3{\cdot}nTHF$ solvate without decomposing borohydride phase. Additionally, the color of THF solution of $NaZn(BH_4)_3$ obtained from mechanochemical synthesis would turn noticeably grey after few hours. These observations are consistent with literature which suggested possible light sensitivity of solvates [10] and the decomposition of $NaZn(BH_4)_3{\cdot}2THF$ solvate into $NaBH_4$ + $Zn(BH_4)_2{\cdot}2THF$ above -25°C while $NaZn(BH_4)_3{\cdot}Et_2O$ solvate remaining stable up to 25°C.

Mikhaeva et al by performing elemental analysis reported that for the chloride-free $NaZn(BH_4)_3{\cdot}nTHF$, molar ratio of $ZnCl_2$ and $NaBH_4$ precursors must be at least 1:4 [6]. Xia et al reported 1:2.5 molar ratio, which means obtained phase is $NaZn(BH_4)_{3-x}Cl_x{\cdot}nTHF$. Additionally, in-situ XRD measurement from the same work shows the formation of NaCl phase at 150°C that is absent in the main phase at RT. This indicates that reported $NaZn(BH_4)_3(NH_3)_2$ phase has non-negligible chloride contamination [7].

Scalable synthesis approach

All the recent synthesis of metal borohydrides and even their ammoniates used ball-milling as a major part of the synthesis process. To achieve potential industrial applications of ammine metal borohydrides (AMB) as solid hydrogen storage materials, their dependency on mechanochemical synthesis must be alleviated.

Solvothermal synthesis technique using liquid ammonia as a solvent enables direct formation of $A_xM(BH_4)_{m+x}(NH_3)_n$ type materials in a single step without the need for ball-milling and other organic solvents. In literature, a typical liquid ammonia synthesis setup involves a quartz reactor of Schlenk line which cannot withstand pressure above 1 bar, hence all the ammonia reactions need to be conducted either at RT as a gas or below -33°C as a liquid [14]. The reaction with ammonia gas cannot exploit solvent properties of ammonia. Some reactions simply cannot be performed due to lower solubility of precursors in other conventional solvents such as THF or dimethyl sulfide. The reaction at -33°C is severely limited in terms of kinetics of the reaction in liquid ammonia as well as lowered solubility. On the other hand, the stainless-steel reactor used for this study can withstand reasonable vapor pressures of liquid ammonia for synthesis well above RT. Hence, it does not suffer from any of the disadvantages described above.

As a summary, the two-step synthesis of AMBs in literature includes the formation and the stabilization of metal borohydrides by ball-milling or as a solvate followed by a reaction with ammonia gas. If we pursued these various approaches for synthesis of various AZBs, the isolation of known $LiZn_2(BH_4)_5$, $Li_2Zn(BH_4)_4{\cdot}Et_2O$, $NaZn(BH_4)_3$, $NaZn_2(BH_4)_5$, $NaZn(BH_4)_3{\cdot}THF$, $KZn(BH_4)_3$ and $K_2Zn(BH_4)_xCl_{4-x}$ phases and their reaction with ammonia gas would create ammoniated main phase and the disproportionation of excess alkali borohydride phases. Additionally, synthesis of these compounds with ZnF_2 precursors is not reported in literature and the reason became obvious from our fruitless trials with conventional solvothermal and ball-milling techniques. Surprisingly, the reaction proceeds very well in liquid ammonia. Utilizing liquid ammonia synthesis technique allowed the synthesis of various AZB compounds with similar crystalline structure and enabled us to investigate the factors that control the release of ammonia impurity during de-hydrogenation process.

2. Material and Methods

2.1. Synthesis procedure

The synthesis process is conducted in liquid ammonia at RT using a stainless steel reactor. The typical stoichiometric synthesis reaction is $ZnX_2 + 3ABH_4 \rightarrow AZn(BH_4)_3(NH_3)_2 + 2AX$ where M = Li; Na; K and X = Cl; F. At standard ambient temperature and pressure conditions, 500 ml of ammonia gas is condensed into small (10 ml) stainless steel reactor containing 300 mg of $ZnCl_2$ (or 230 mg of ZnF_2) and corresponding amount of alkali borohydride (Table 1) precursors followed by magnetic stirring at 350 rpm. The typical synthesis duration of 24 hours is sufficient for $LiZn(BH_4)_3(NH_3)_2$ and $NaZn(BH_4)_3(NH_3)_2$ compounds while $KZn(BH_4)_3(NH_3)_2$ compounds require up to one week due to lower reactivity and solubility (Table S1). The complete evaporation of ammonia solvent is most difficult for $LiZn(BH_4)_3(NH_3)_2$ compound which requires up to 24 hours under dynamic vacuum.

The synthesis of mono-metallic $Zn(BH_4)_2(NH_3)_2$ in liquid ammonia though possible was not reproducible. Instead, formation of bimetallic phase is preferred even with $ZnCl_2$:ABH_4 ratio of 1:2 or lower, where $[BH_4]^-$ sites in the main phase are substituted with Cl^- anions to compensate for the deficiency of ABH_4. Hence, synthesis of $Zn(BH_4)_2(NH_3)_2$ is performed in two steps. Initially, $Zn(NH_3)_2Cl_2$ precursor prepared by introducing $ZnCl_2$ into ammonia in THF solution. The second step is the reaction of this precursor with $LiBH_4$ in 1:2 ratio in THF using the Schlenk reactor. However, the kinetics of the reaction is rather slow requiring at least 10 days to complete and delivers a product with poor crystallinity. The evaporation and complete removal of THF from the final product requires at least 48 hours under dynamic vacuum. In all cases white powder needs to be obtained, any grey color indicates the partial decomposition and reduction of zinc precursor. Hence, for this study we chose to also reproduce the synthesis process described in reference [11]. $Zn(NH_3)_2Cl_2$ precursor ball-milled with 2 moles of $LiBH_4$ in Retsch Emax. Ball-mill jar of 125 ml was filled with 30 steel ball (10 mm diameter) and the precursor added in ball-to-powder ratio of 155. The rotation speed was set to 500 rpm and pause steps to 2-minute interval while the ball-milling jar was cooled actively to 10°C. The total duration of the synthesis was 2.5 hours.

Table 1: Summary of synthesized samples

Short name	Main phase	Precursors	Molar ratio	Byproduct	Estimated **x** value
c-ZnAB	$Zn(BH_4)_{2-x}Cl_x(NH_3)_2$	$Zn(NH_3)_2Cl_2 : LiBH_4$	1 : 2	LiCl	0 (0%)
c-LiZnAB	$LiZn(BH_4)_{3-x}Cl_x(NH_3)_2$	$ZnCl_2 : LiBH_4$	1 : 2.5	LiCl	0.5 (16%)
c-NaZnAB	$NaZn(BH_4)_{3-x}Cl_x(NH_3)_2$	$ZnCl_2 : NaBH_4$	1 : 2.3	NaCl	0.7 (23%)
c-KZnAB	$KZn(BH_4)_{3-x}Cl_x(NH_3)_2$	$ZnCl_2 : KBH_4$	1 : 2	KCl	1 (33%)
f-NaZnAB	$NaZn(BH_4)_{3-x}F_x(NH_3)_2$	$ZnF_2 : NaBH_4$	1 : 2.3	NaF	0.7 (23%)

f-KZnAB	$KZn(BH_4)_{3-x}F_x(NH_3)_2$	ZnF_2 : KBH_4	1 : 1.2	K_2ZnF_4	1.5 (50%)

Anhydrous $ZnCl_2$ (99.995%), $NaBH_4$ (99.99%), KBH_4 (98%), NH_4Cl (99.5%) and $NaNH_2$ (98%) precursors were purchased from Sigma Aldrich while $LiBH_4$ (95%) from Fluka and ZnF_2 (95%) from Acros Organics. Anhydrous ammonia gas is generated by heating the $NaNH_2$-NH_4Cl mixture to 150°C. The precursors and products are handled in air-free manner under high purity argon atmosphere of glovebox and Schlenk line.
In the following sections, the synthesized samples are referred by their "short name" indicated in Table 1. The precursor ratio described in this table was experimentally determined in order to minimize the unreacted precursors and optimize the yield of the reaction where "the main phase" and the corresponding alkali halide "byproduct" are the main reaction products. The estimated anion substitution degree (x) is calculated (Equation S1) based on precursor ratio and the formula of main products. These estimations as well as the percentage of substituted boron sites are summarized in Table 1.

2.2. Computational technique

First-principle calculations were carried out using density functional theory method implemented in Quantum Espresso (QE) package [15]. Exchange and correlation were treated in the generalized gradient approximation (GGA) of Perdew, Burke and Ernzerhof (PBE) based on standard ultra-soft and Projector-Augmented Wave (PAW) pseudopotentials of Quantum Espresso package. "Grimme-D3" implementation of QE is used to account for "dispersion correction" in bonding energy. PAW pseudopotentials with kinetic energy cutoff of 110Ry and the charge density cutoff of 600Ry were used for the structural optimization and GIPAW NMR chemical shift calculations [16]. For all the other calculations, the ultrasoft pseudopotentials with a kinetic energy cutoff of 60 Ry are chosen. The precision threshold for electronic energy calculation were set below $1x10^{-10}$ Ry. Brillouin-zone was sampled with k-point grid of maximum 0.33 $Å^{-1}$ density.

Application of ab-initio molecular dynamics (AIMD) to the analysis of vacancy formation [17] inspired us to analyze the likelihood of halide substitution or alkali borohydride vacancies in the crystalline structure of AZB compounds. The same crystalline lattice parameters (a = 7.2965 Å, b = 10.1444 Å and c = 12.9714 Å) were used for all the bimetallic phases (100 atoms) while 3x1x1 super lattice (a = 19.1772 Å, b = 8.4176 Å, c = 6.3884 Å, β = 92.407°) were used for monometallic phase (152 atoms) to have exactly 12 borohydride anions in the unit cell for all the phases. The defects were created by either replacing one $[BH_4]^-$ site (~8% of 12 available sites in super cell) with a halide (Cl^- or F^-) anion or by removing one $[BH_4]^-$ as well as accompanying alkali cation (A^+) to preserve the electroneutrality. Without modifying the Bravais lattice type, the unit cell parameters and atomic positions were optimized with simulated 300K temperature control mechanism based on periodic rescaling of the velocities of the atoms. Time step used for these calculations is 0.5 femto-seconds. To minimize noise and uncertainty inherent to molecular dynamics, further variable cell optimization were performed without temperature factor. BFGS method is used when available with 0.5 kbar convergence limit of pressure for unit cell parameter optimization.

It is well established that AMBs decompose in melted viscous state. The de-hydrogenation and de-ammoniation reactions start once the necessary energy is spent to destabilize the crystalline dihydrogen bond network. To emulate this melted viscous state, one formula unit of $AZn(BH_4)_3(NH_3)_2$ (where A = ZnH, Li, Na, K) was placed in a cubic cell with a lattice parameter

of 20 Å (model is adopted from reference [18]). The positions of the atoms were optimized using the BFGS method until the residual forces were less than $1x10^{-4}$ Ry/Bohr.

2.3. Characterization techniques

Powder X-ray Diffraction (XRD) measurements were conducted using sample holders with dome-shaped airtight covers on a commercial Bruker D8 Discover diffractometer operating using Cu Kα radiation and equipped with a 1D LynxEye XE-T detector. Le Bail and Rietveld refinement analysis using HighScore and Fullprof softwares were performed considering pseudo-voigt peak profile function and Chebyshev polynomial to account for the background. The standard deviation in unit cell volume is calculated by manually changing unit cell parameters until the goodness of fit started to increase.

Thermogravimetric analysis (TGA) and Mass Spectroscopy (MS) measurements performed simultaneously (Netzsch STA 449 - QMS 403C) under argon flow and heating rate of 10 °C min^{-1}. Simultaneous Differential Scanning Calorimetry (DSC) and TGA measurements performed using Setaram Sensys Evo under helium flow and heating rate of 2 °C min^{-1}. All experiments were performed using aluminum crucibles with an aluminum cap which restricted sample exposure to air during transfer from glovebox. A small hole on the cap helps to avoid overpressure during de-hydrogenation.

The volumetric desorption (PCT) experiments were conducted using Sievert type Setaram PCT Pro. The sample decomposition process was performed under constant heating rate and initial 1 bar of hydrogen atmosphere was applied to emulate similar experimental conditions to TGA (under 1bar of He flow). The released ammonia and hydrogen quantity are calculated by combining TGA and PCT results:

$$\Delta P_{PCT} = R\frac{T_{PCT}}{V_{PCT}}(n_{H_2} + n_{NH_3})$$

$$\Delta m_{TGA} = \left(\frac{m_{TGA}}{m_{PCT}}\right)(n_{H_2}M_{H_2} + n_{NH_3}M_{NH_3})$$

Δm_{TGA} is the weight loss measured by TGA while m_{TGA} is the initial mass of the sample, similarly m_{PCT} is the initial mass of the same sample used in PCT measurement. n_i and M_i are the molar quantity and the molar mass of the gases released during decomposition that result in pressure increase of ΔP_{PCT} in known V_{PCT} volume.

The Raman spectroscopic analysis was conducted by confocal Raman microscope (Renishaw) using airtight sample holder with a thin glass window transparent to 633 nm red laser. The sample holder was precooled to 5°C and wide beam spot is used to avoid decomposition of sample due to laser heating.

High-resolution solid-state ^{11}B and ^{1}H NMR spectra were recorded with a 4 mm Bruker CPMAS probe head on a Bruker AVANCE III DSX 500 spectrometer with an 11.74 T magnet operating at 160.4 MHz for the ^{11}B, and 500.18 MHz for the ^{1}H. The 4 mm (92 µL) diameter cylindrical double bearing rotors made of zirconia were used with specific airtight Teflon inserts. Experimental referencing, calibration, and setup were done using solid powder sodium borohydride, $NaBH_4$, its chemical shift of -42.06 ppm relative to the primary standard, liquid $F_3B{\cdot}O(C_2H_5)_2$ (where $\delta(^{11}B)$ is set to 0.00 ppm). The probe exhibits a small, but manageable background ^{11}B signal due to boron nitride in the stators. The Hahn echo pulse sequence was

generally effective at suppressing the background signal. ^{1}H NMR signals were acquired either with direct excitation or Hahn echos. Proton decoupling was applied during the acquisition of the FIDs. MAS spinning frequencies was generally set to 12 kHz. Data were processed using TopSpin 3.6.

3. Results

Four different AZB compounds were synthesized. As already mentioned, $Zn(BH_4)_2(NH_3)_2$ and $NaZn(BH_4)_3(NH_3)_2$ have been previously reported ([11],[7]) while we were able to synthesize $LiZn(BH_4)_3(NH_3)_2$ and $KZn(BH_4)_3(NH_3)_2$ compounds for the first time. $NaZn(BH_4)_3(NH_3)_2$ and $KZn(BH_4)_3(NH_3)_2$ compounds were also alternatively synthesized using $ZnCl_2$ and ZnF_2 precursors. It was not possible to synthesize $Zn(BH_4)_2(NH_3)_2$ and $LiZn(BH_4)_3(NH_3)_2$ compounds with ZnF_2 precursor.

3.1. Structural analysis

The structural properties of the different synthesized compounds were investigated by means of XRD. The obtained results are presented in Figures S1-S6. Depending on the precursors alongside the main alkali halide byproduct phases (LiCl, NaCl, KCl, NaF, K_2ZnF_4) small amount of unreacted precursors ($NaBH_4$, KBH_4, ZnF_2, $Zn(NH_3)_2Cl_2$) can be observed besides the main phase. LeBail profile refinements of XRD data were performed in order to determine the lattice parameters as well as microstructure of the AZB phases. Table 2 presents the values of the obtained lattice parameters and the strain ε_0 determined considering distortion broadening only. $Zn(BH_4)_2(NH_3)_2$ has $P2_1$ space group as reported in reference [11]. The rest are bimetallic AZB phases which are all isomorphic having the same orthorhombic structure with $P2_1nb$ symmetry, as previously identified for $NaZn(BH_4)_3(NH_3)_2$ [7]. Surprisingly, c-LiZnAB, c-NaZnAB, f-NaZnAB and f-KZnAB display very close unit cell volumes of $958\pm4 Å^3$ within the precision of LeBail fitting analysis (Figure 2a). The c-KZnAB compound differs from the other compounds with a unit cell volume smaller by about ~9%. This compound is also characterized by the highest value for the distortion parameter ε_0. For all the probed compounds, the lattice is appeared to be dominated by strain (distortion) effect, with crystallite sizes larger than 150 nm. With the aim of getting more information on the structure of the AZB phases, more precisely concerning the atomic site occupancies and eventual substitutions, we performed Rietveld refinement analysis based on the structure published by Xia et al. [6]. However their structure determination, which was based on powder X-Ray diffraction data, did not allow the estimation of the values of the Debye-Waller factors (DW) for the different atomic sites. Only one isotropic displacement factor was refined for all the atoms, which is clearly unrealistic considering the differences in local coordination for the different atomic sites. The influences of atomic thermal vibrations and site occupancies on the diffraction pattern being strongly coupled, the fact of not knowing the DW values, therefore made reliable determination of the site occupancies and substitutions impossible. Fortunately, NMR spectroscopy has proven to be a very valuable tool to provide information on these aspects.

Table 2: Summary of structural parameters of AZBs

	a (Å)	b (Å)	c (Å)	β (°)	V(Å^3)	ε(%)	Rwp
c-ZnAB	6.42	8.46	6.42	92.36	348.4	0.10	3.6
c-LiZnAB	7.29	10.14	12.97	90.00	958.7	0.09	6.1
c-NaZnAB	7.28	10.13	12.93	90.00	953.5	0.14	4.7
f-NaZnAB	7.30	10.15	12.97	90.00	961.0	0.08	5.8
c-KZnAB	7.09	9.90	12.51	90.00	878.0	0.23	3.9
f-KZnAB	7.29	10.14	12.96	90.00	958.0	0.10	5.8

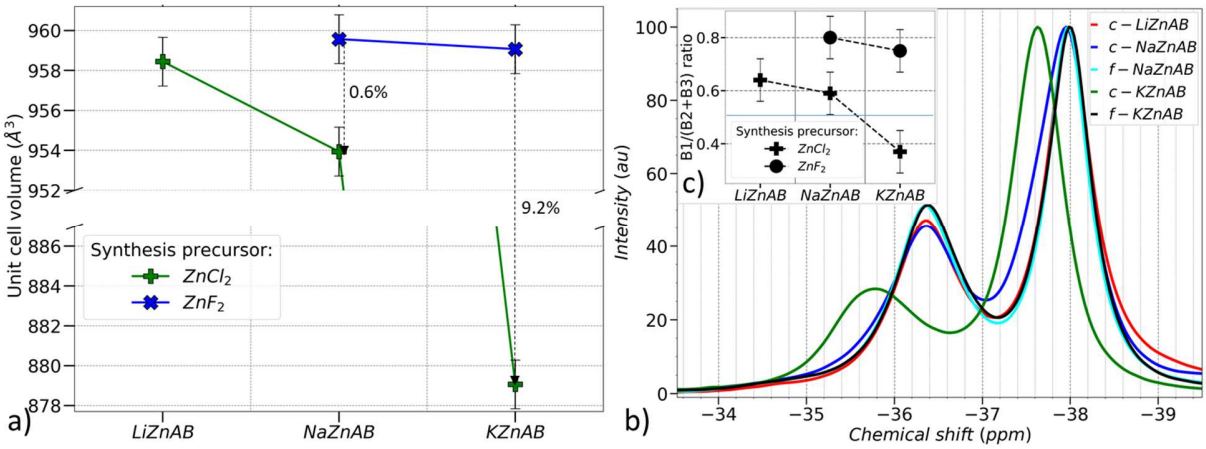

Figure 1: a) Unit cell volume comparison for all bimetallic AZB compounds synthesized from $ZnCl_2$ and ZnF_2 precursors b) ^{11}B MAS NMR spectra of bimetallic AZB compounds synthesized with $ZnCl_2$ precursors c) ^{11}B MAS NMR peak area ratio of single to double B1/(B2+B3) boron sites

As mentioned, almost identical unit cell volume for bimetallic AZB compounds (except c-KZnAB) is very surprising result. One explanation is that crystallographic site for alkali cation is big enough to accommodate even K^+ cation. Another possibility is due to the existence of potentially higher amount of fluoride substitution or alkali borohydride vacancies in f-KZnAB compared to f-NaZnAB which would compensate for larger potassium cation. As it can be seen from Figure 1a (green line), for bimetallic AZB compounds synthesized with $ZnCl_2$ precursor, the c-KZnAB has the smallest unit cell volume while c-LiZnAB has the biggest unit cell volume. As the ranking of alkali cation ionic radii is $r(K^+) > r(Na^+) > r(Li^+)$, the only possible explanation for inverse relationship in unit cell volume was that the impact of anion substitution effect ($[BH_4]^- \rightarrow Cl^-$) dominating over the cation replacement effect. Since ionic radius of Cl^- is smaller than that of $[BH_4]^-$, this means that the degree of anion substitution increases as we move from lithium to potassium compound. This is also evident from precursor ratio necessary to obtain the highest yield for the main phase and the corresponding byproduct (Table 1).

Fortunately, more substantive information can be obtained using NMR spectroscopy. The c-ZnAB sample has a single peak at 43.5 ppm (Figure S9) which corresponds to single type of boron site namely boron atoms which are the ligands of Zn tetrahedra. Conversely, bimetallic AZB compounds show two distinct chemical sites for boron atoms within the structure. For c-LiZnAB higher intensity peak is at 37.9 ppm while lower intensity peak is at 36.4 ppm (Figure1b). These values are exactly the same for f-NaZnAB and f-KZnAB compounds. This result points to the overall enhanced electronic shielding due to alkali cations in bimetallic compounds compared to c-ZnAB. But within the bimetallic compounds there is a minimal difference. Similarly, the chemical shift due to the varying degree of halide anion substitution is non-existent. The only observed correlation is the lower chemical shift with lower unit cell volume (c-NaZnAB and c-KZnAB in Figure 2a). The double boron peak in ^{11}B NMR of bimetallic compounds can be explained from the crystalline structure (Figure S7) where two boron sites (B2 and B3) which constitute the edges of the zinc tetrahedra are closer to both alkali and zinc cations while the third boron site (B1) has longer bonding lengths with both cations. Hence, in ideal compound the ratio of the areas of NMR peaks should be 0.5. This can be confirmed by fitting the peaks with pseudo-Voigt profile, resolving the peaks and looking at the ratio of the area of two ^{11}B NMR peaks. In Figure1c, the area ratio of two peaks is plotted for each AZB compound. One shortcoming of this analysis is that we can only see the relative concentration

of boron atoms in B1 and B2/B3 sites. ^{11}B NMR spectroscopy cannot determine whether these sites are substituted by halide anion or left vacant. Hence, we can conclude that defect concentration is higher in B1 site compared to B2/B3 sites in c-KZnAB compound. On the other hand, compounds synthesized with ZnF_2 precursor have higher defect concentration in B2/B3 boron sites.

XRD and NMR results, which leave important issues open, were complemented by DFT calculations. As shown for crystalline ammonia borane, to correctly predict the dihydrogen network behavior using DFT calculations, the Van-der Waals interactions (semi-empirical method proposed by Grimme [19]) need to be taken into account [20]. It was found that using a multiplication factor of 1.05, 1.05, and 1.30 for B, N, and H atomic radii, provided the best agreement with experimental crystalline structure. However this approach was not effective for bimetallic AZBs. Our structural optimization efforts with or without "dispersion correction", using ultrasoft or PAW pseudopotentials showed that the described structure in reference [7] is not stable. More precisely, the alkali cations in the structure are far from energetic minima. Nevertheless, a positive correlation of the optimized unit cell volume with alkali cation size is clearly observed. The calculated unit cell volume for $AZn(BH_4)_3(NH_3)_2$ phases for A=Li, Na, K are 887, 928 and 978 Å^3, respectively (Table S3). Given that the experimental value is around 960 Å^3 (Table 2 – except c-KZnAB), we can conclude that crystallographic site for alkali cation is big enough to accommodate even K^+ cation. Due to the extreme sensitivity of GIPAW calculations to crystalline structure, the calculated chemical shift values do not have high enough precision. Nevertheless, these values confirm our interpretation of the experimentally observed two NMR peaks with up- and downshifted peaks respectively corresponding to B1 and B2/B3 sites (Figure S8). On the other hand, DFT optimized structure for $Zn(BH_4)_2(NH_3)_2$ phase agrees remarkably well with experimental unit cell parameters and unit cell volume (Table S3). Additionally, GIPAW NMR chemical shift calculations helped to confirm that B2 and B3 sites are identical with calculated -45.2±0.1 ppm chemical shift compared to single peak observed in ^{11}B NMR at -43.5 ppm (Figure S9).

Further variable cell AIMD calculations were performed to evaluate likelihood of vacancies formation and anion substitution processes. The major advantage of this approach is the ability to periodically create and break many possible combinations of "dihydrogen network" and avoid local energetic minima [21] (Figure S10-S13). The energy of formation of defects is calculated as:

$$\Delta E_{vacancy} = [E_{structure\text{-}ABH4}(crys) + E_{ABH4}(crys)] - E_{structure}(crys)$$

$$\Delta E_{substitution} = [E_{structure\text{-}BH4+X}(crys) + E_{HZnBH4}(gas)] - [E_{structure}(crys) + E_{HZnX}(gas)]$$

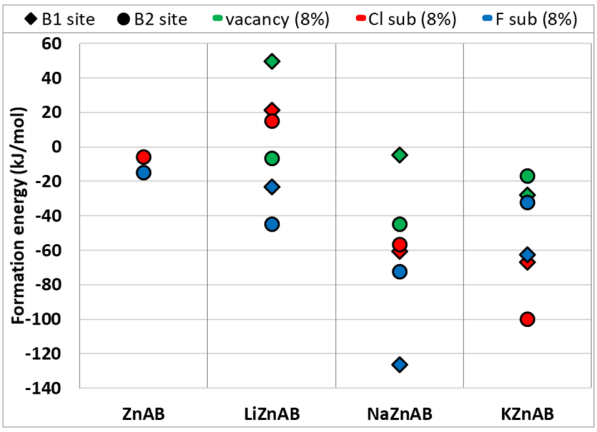

Figure 2: a) The calculated enthalpy of formation of alkali borohydride vacancies and halide substitutions in AZB compounds (after variable cell AIMD followed by relaxation calculations)

As shown in Figure 2, the alkali borohydride vacancy formation is energetically less favorable to halide substitution for all phases. Hence, we can conclude that in the presence of halide anions the vacancy formation is not likely. Additionally, Figure 2 also shows that the chloride anion substitution is less probable in ZnAB and LiZnAB compounds. Considering also that we were not able to synthesize these compounds with ZnF_2 precursor, our computational model agrees well with the fact that c-LiZnAB and c-ZnAB also have the lowest defect concentration (Table 1). Beyond determining the likelihood of defect formation, the real concentration of defects can only be measured by experimental characterization. However, in our case, the degree of anion substitution could only be inferred from the optimum precursor ratio (Table 1). Hence, determining the equilibrium concentration of defects is out of the scope of this study. Additionally, in practice the equilibrium concentration of the defects depends on the solubility of the precursors and the products in the reaction medium (Table S1). Nevertheless, considering the different ionic radii (Table S2) of alkali cations and halide anions as well as their different equilibrium concentrations, the reason for c-LiZnAB, f-NaZnAB and f-KZnAB having similar unit cell parameters remains unknown. Additionally, it is difficult to explain the unit cell contraction due to chloride anion substitution while fluoride anions have even smaller ionic radii.

Solvothermal synthesis of metal borohydrides by salt metathesis reaction in THF is known to produce ammonia borane type impurities in addition to the main phase [14]. Therefore, it was important to ensure the absence of NH_3BH_3 like impurities in our samples. Figure 3 shows Raman spectra of AZBs as well as NH_3BH_3 as a reference. The N-H and B-H stretching modes are common in all of these compounds. However, more importantly unlike ammonia borane, B-N stretching mode (780 cm^{-1}) is absent in AZB compounds. Additionally, they all have a strong vibrational mode present at ~420 cm^{-1} which has been previously attributed to Zn-B stretching mode in zinc borohydride compounds [22],[23]. These results confirm the purity of the synthesized AZB compounds.

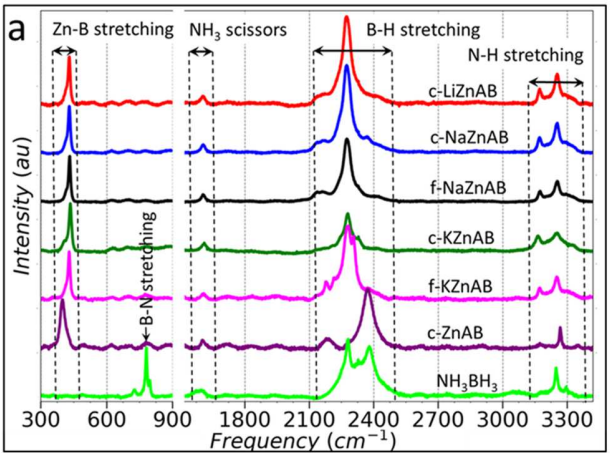

Figure 3: Raman spectra of all the AZB compounds compared to NH_3BH_3

Splitting of B-H stretching Raman peaks in ammonia borane is assigned as asymmetric stretching mode for higher frequency region and symmetric stretching mode for the lower frequency range [24]. The c-ZnAB sample has similar splitting in B-H stretching vibrational modes as previously reported in metal borohydrides, representing bidentate (two M-H-B bridges) or tridentate (three M-H-B bridges) bonding structure [25]. As evidence to the presence of $[M(BH_4)_m]^{m+}$ complex anions in the structure the higher frequency peaks are tentatively attributed to outward stretching B-H bond while lower frequency peaks to inwards stretching modes [26]. The intensity ratio of these peaks are used to differentiate between bidentate and tridentate structure [22]. An identical reasoning leads to the conclusion that $Zn(BH_4)_2(NH_3)_2$ has monodentate structure (single Zn-H-B bridge). This is also supported by vibrational frequency of the main peak which is in the 2300-2450 cm^{-1} range. Same argument is applicable for bimetallic AZB compounds as well, however the main peak is shifted to 2200-2350 cm^{-1} range. For tetrahedral geometry of metal cation, this range is attributed to ionic structure similar to $Mg(BH_4)_2$ [27]. The peak center of 2280 cm^{-1} corresponds exactly to the value reported for $Mg(BH_4)_3(NH_3)_6$. Conversely, the splitting of B-H vibrational modes in $Li_2Mg(BH_4)_4(NH_3)_6$ is attributed to the formation of $[Li_2(BH_4)_4]^{2-}$ complex anion [28]. This explanation also agrees well with $AZn(BH_4)_3(NH_3)_2$ compounds since no complex ion exists in the structure. For alkali borohydrides, increasing cation size is ascribed to B-H bond lengthening. This translates to lowering of vibrational frequency for stretching mode [27]. Hence, lower frequency of Zn-B stretching mode tells us that Zn-B bonding length is longer in monometallic $Zn(BH_4)_2(NH_3)_2$ compared to bimetallic $NaZn(BH_4)_3(NH_3)_2$, which is confirmed by the crystal structure (2.28 Å vs 2.12 Å) (supplementary information from references [7] and [11]). Changes in multiples of N-H stretching modes are also ascribed to local symmetry change of M-NH_3 group in the crystalline structure [29]. As a conclusion, Raman spectra of AZB compounds reveal that despite the presence of same zinc tetrahedra in all the compounds, various bonding energies between monometallic and bimetallic compounds are distinctly different while the effects of alkali cations in bimetallic compounds are minimal. DFT computational cost of vibrational frequencies in crystalline structure was too high, hence we relied heavily on interpretations from other literature.

In AMBs, the ammonia molecules in general prefer to coordinate to higher electronegativity metals, while the borohydride anions prefer to bond with lower electronegativity metals. The hypothesis for this study is that introducing an alkali cation in close proximity of zinc tetrahedra and tuning its electronegativity will enable the tuning of the bonding lengths and strengths which should affect the decomposition process. In order to understand the de-hydrogenation process

of AMBs, unlike comparing various AMBs to each other, this set of similar zinc compounds (Table 1) provides a unique opportunity to minimize independent parameters (such as crystalline structure, number of ammonia adducts and properties of the main metal cation). Although the $Zn(BH_4)_2(NH_3)_2$ compound has different crystalline structure, on atomic level it is still very similar to bimetallic compounds. In all of these AZB compounds, zinc cation seats in the center of the tetrahedra and coordinates by two ammonia as well as two borohydride ligands. Therefore, a bimetallic phase consists of this zinc tetrahedra with an additional alkali borohydride in its vicinity, $AZn(BH_4)_3(NH_3)_2 = Zn(BH_4)_2(NH_3)_2 + ABH_4$.

3.2. Thermodynamic analysis

All AZBs upon heating decompose in two steps: a broad shallow endothermal peak quickly followed by sharp exothermal peak (example of DSC-TGA result for each sample is given in Figures S14-S19). The endothermal peak corresponds to melting process which is the energy necessary to break the dihydrogen bonding network [11]. Meanwhile, the sharp exothermal peak can be explained by "dihydrogen elimination" reaction. The on-set and off-set temperatures of both endothermal and exothermal peaks of all compounds are plotted in Figure 4a. The first observation in accordance with literature is that the thermal stabilization of compounds is mainly due to the Cl^- anion substitution [13]. Hence, the effects of alkali cation replacement or fluoride anion substitution on the decomposition temperature is almost negligible. Lower temperature of exothermal peak in c-ZnAB indicates possibly different de-hydrogenation mechanism compared to bimetallic phases.

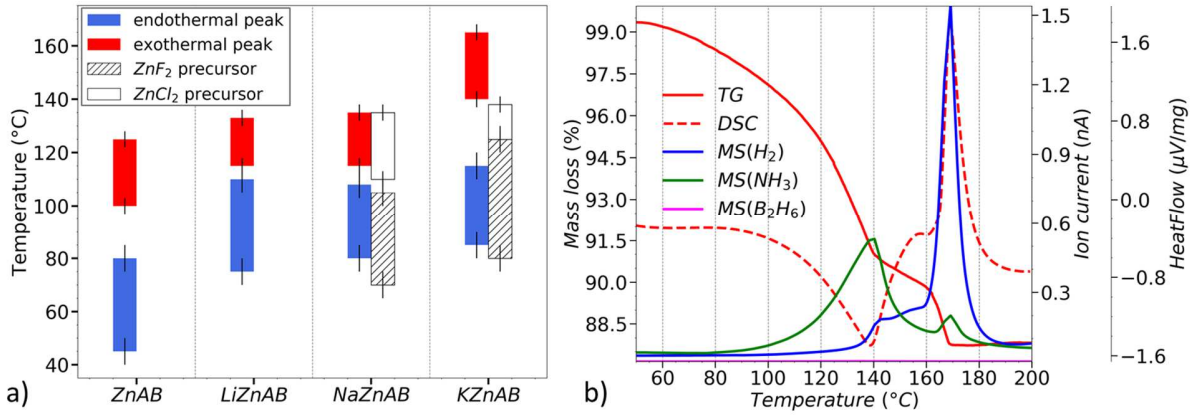

Figure 4: a) On-set and off-set temperatures (bottom and top of the bar) of endothermal (blue) and exothermal (red) peaks for the compounds synthesized with $ZnCl_2$ precursors (solid fill) and ZnF_2 precursor (dashed fill). The heating rate is 2°C/min. b) TGA-MS analysis of c-KZnAB sample (10°C/min heating rate)

The TGA-MS analysis of c-KZnAB sample has sufficiently resolved peaks and a clear mass loss corresponding to the endothermal peak (Figure 4b). More precisely, this peak can be associated with the melting triggered "evaporation of excess ammonia". Basically, ammonia molecule surrounded by high concentration of halide anions cannot participate in de-hydrogenation reaction. Once the melting process is completed, the de-hydrogenation process starts (blue line in Figure 4b). However, there is a second de-ammoniation process that occurs simultaneously with exothermal de-hydrogenation peak. This de-ammoniation process is in competition with de-hydrogenation processes. Additionally, for all the AZB compounds except c-KZnAB, the exothermal decomposition process happens in 100-140°C temperature range. Since this decomposition step takes place in a melted viscous state, a more in-depth understanding of the decomposition process is needed to explain these phenomena.

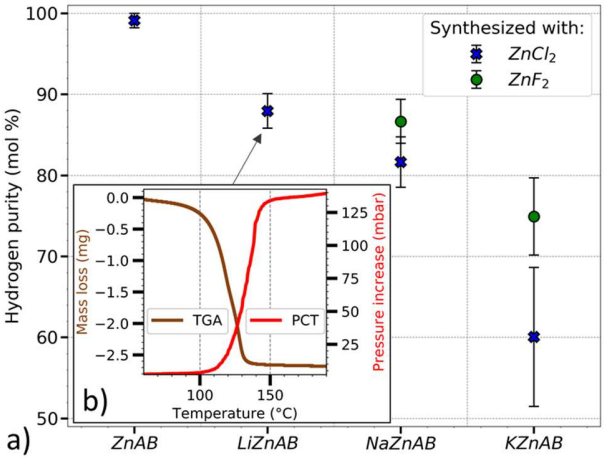

Figure 5: a) Calculated H_2 purity of each compound synthesized with $ZnCl_2$ (green ●) and ZnF_2 (blue ×) precursors b) TGA (brown) and PCT (red) measurements of c-LiZnAB sample (25°C/min and 10°C/min heating rate, respectively)

To further understand the differences in the decomposition processes of AZB compounds, we quantify the released gases. Hence, the molar percentage of released hydrogen is calculated for all compounds and the results plotted in Figure 5a. An example of TGA and PCT measurements necessary for this calculation is shown for c-LiZnAB in Figure 5b. A clear tendency emerges, the ammonia release from AZB compounds increases with decreasing average cation electronegativity. Additionally, bimetallic AZB phases with fluoride substitution release lower amount of ammonia impurity.

With varying degree of halide anion substitution in synthesized samples, the effects of alkali cation vs halide anion cannot be completely isolated. Hence, a computational approach is employed to answer this question. First, the structure of $AZn(BH_4)_3(NH_3)_2$ molecule optimized for A = ZnH, Li, Na and K species. Similar optimizations performed again, once an ammonia or a hydrogen molecule removed from the initial structure. The enthalpy of formation for the chosen vacancy is calculated as:

$$\Delta E_{formation} = [E_{strucure\text{-}vacancy}(gas) + E_{molecule}(gas)] - E_{structure}(gas)$$

In Figure 6a, the optimized final structure is depicted for the de-ammoniation as well as two types of energetically most favorable “dihydrogen elimination” reactions. Additionally, B1 and B2 borohydride sites were replaced with fluoride or chloride anions to study their effects on de-hydrogenation and de-ammoniation reactions. It is important to note that we did not investigate the energetic barrier due to the transition states between initial and final structures. However, in melted state we assume that this energetic barrier would be negligible.

Alternative de-hydrogenation reactions through formation of diborane, hydrazine or ammonia borane like species were explored as well and found to be energetically very costly. Hence, energetically most favorable two “dihydrogen elimination” reactions are:

- “ZnN-(H2)-BZn” → between protic hydrogen of ammonia molecules and the hydridic hydrogen of borohydride species polarized by zinc cations,
- “ZnN-(H2)-BA” → between protic hydrogen of ammonia molecules polarized by zinc cations and the hydridic hydrogen of borohydride species polarized by alkali cations.

For every AZB compound with or without halide substitution, we observe following order in reaction enthalpy “ZnN-(H2)-BA” < “ZnN-(H2)-BZn” < “ZnN-(NH3)-BA” (Figure 6b). As shown in

Figure 6b, all reactions are endothermal which is expected as these DFT calculations do not take into account the temperature factor and thermal energy (heating above 100°C) is necessary to initiate these decomposition reactions.

De-hydrogenation reactions (green and orange colors in Figure 6b) require more energy while de-ammoniation reaction (purple color in Figure 6b) needs less energy as we move from ZnAB towards KZnAB. Ammonia impurity relationship we observed in Figure 5a can be more easily explained by enthalpy difference between de-ammoniation and two types of de-hydrogenation reactions, plotted in Figure 6c. Once the necessary thermal energy provided and de-hydrogenation process starts, KZnAB requires the least amount of energy to release ammonia. Meanwhile, the same energy barrier for de-ammoniation is the highest for ZnAB compound. As a conclusion, irrespective of the halide substitution, the alkali cation with higher electronegativity will result in higher hydrogen purity during decomposition of AZB compounds.

The preferential substitution of boron sites is also very consequential for ammonia impurity as well. As shown in Figure 6c, any halide substitution of B2 site suppresses ammonia release while supporting the "ZnN-(H2)-BA" de-hydrogenation reaction. On the other hand, the major consequence of anion substitution of B1 site is the elimination of this reaction pathway. If all the B1 sites substituted with halides, zinc tetrahedra will be surrounded by unreactive alkali halides forcing the energetically less favorable "ZnN-(H2)-BZn" de-hydrogenation pathway to become dominant. DFT calculations provide additional supports for this hypothesis, for NaZnAB and KZnAB compounds, the halide substitution of B1 site also lowers "de-ammoniation barrier" (green arrow down in Figure 6c). On the other hand, the substitution of B2 site increases "de-ammoniation barrier" for all compounds (red arrow up in Figure 6c). Finally, taking into account ^{11}B NMR analysis for preferential substitution of boron sites (Figure 1c), f-KZnAB with mostly B2/B3 sites occupied with fluoride anions will benefit from energetically more favorable "ZnN-(H2)-BK" reaction. Conversely, c-KZnAB with B1 sites mostly blocked by chloride anions will be forced to rely on energetically less favorable "ZnN-(H2)-BZn" reaction, meanwhile having lower "de-ammoniation barrier". Therefore, this hypothesis also helps to explain higher on-set temperature of exothermal decomposition peak of c-KZnAB observed in DSC measurements (Figure 3a). Notably, this type of blocking mechanism is not applicable for $Zn(BH_4)_2(NH_3)_2$ (no B1 sites). The absolute reaction enthalpy numbers might change with the precision of DFT calculations as well as with the limitations and assumption considered for the DFT model. Notably, we should not forget that the energy calculations are for the gaseous phase. Nonetheless, despite all the assumptions, the correlation between experimental and computational results is conclusive.

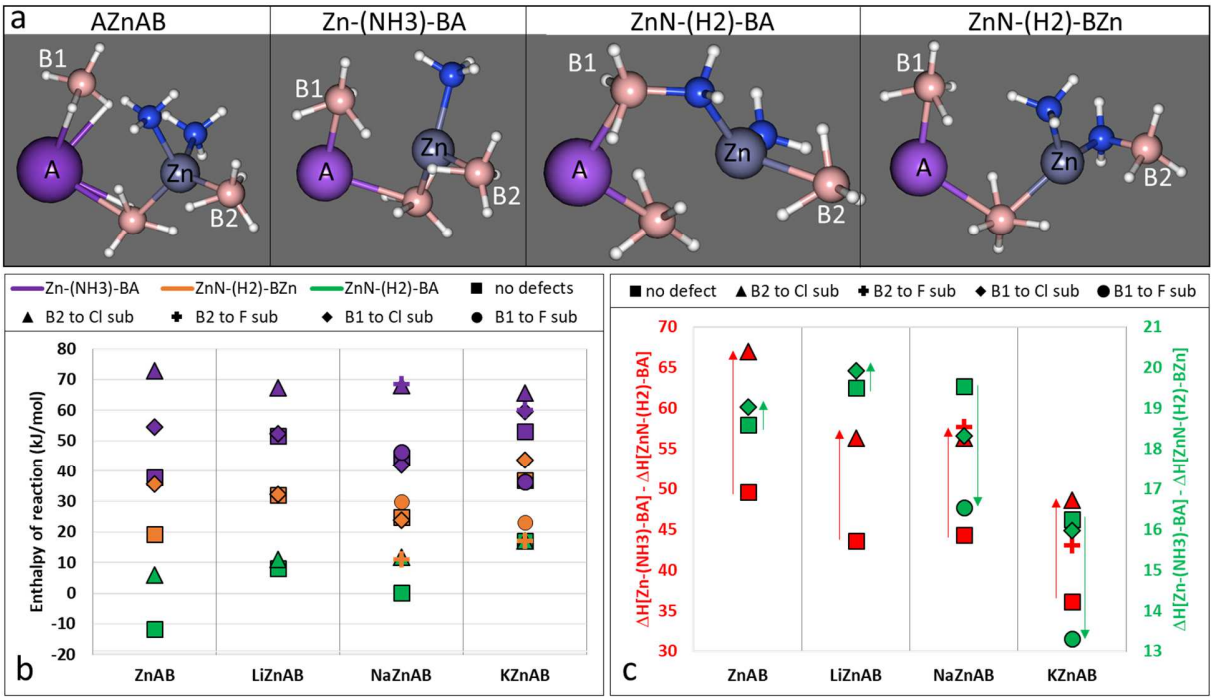

Figure 6: a) visual description of decomposition reactions considered for DFT calculations b) calculated enthalpy of these decomposition reactions c) enthalpy difference between de-ammoniation and de-hydrogenation reactions for each case of alkali cation A= ZnH, Li, Na, K as well as Cl^- and F^- substitution of B1 and B2 boron sites

4. Discussion

Two new ammine borohydride compounds are synthesized and reported in this article for the first time. $LiZn(BH_4)_3(NH_3)_2$ is the ideal example for demonstrating the sensitivity of synthesis technique and conditions in order to obtain the desired compound. Despite being more stable than $Zn(BH_4)_2(NH_3)_2$ phase, $LiZn(BH_4)_3(NH_3)_2$ cannot be synthesized neither by ball-milling $Zn(NH_3)_2Cl_2$ and $LiBH_4$ [11] nor by solvothermal synthesis in organic solvents. Additionally, ball-milling $ZnCl_2$ and $LiBH_4$ precursors results in formation of $LiZn_2(BH_4)_5$ phase since $LiZn(BH_4)_3$ is unstable. Without stabilizing $LiZn(BH_4)_3$, the reaction with ammonia gas is also not possible. Hence the only route to $LiZn(BH_4)_3(NH_3)_2$ formation is direct synthesis using liquid ammonia as a solvent. We tried to replicate metathesis reaction between ZnF_2 and KBH_4 using THF assisted ball-milling technique, after several attempts with different ball-to-powder ratio, and synthesis duration at 500rpm no evidence of reactions between the precursors could be observed. Hence, the only option is liquid ammonia synthesis.

In this study, identical crystallographic structure of $AZn(BH_4)_3(NH_3)_2$ compounds allowed us to replace alkali cation from Li^+ to Na^+ to K^+ without modifying zinc tetrahedral building block. We have also successfully demonstrated that halide anion substitution of borohydride sites has major effect on the ammonia impurity which cannot be avoided when salt metathesis reaction is used in solvothermal synthesis.

The computational studies in literature identified various decomposition pathways that AMBs take upon heating. Direct “dihydrogen elimination” process in a given AMB depends on relative charge of H atoms in BH_4 and NH_3 molecules (calculated as Brader charge) as well as local geometry of hydrogen bond network. This reaction alone does not explain the whole decomposition process. These compounds also benefit from $[B_2H_7]^-$ formation that might react

with NH_3 to form NH_3BH_3 intermediate species and release more hydrogen [30]. Additionally, intermediate reactions which are more exothermal can have significant effect of the purity of the released hydrogen. These reactions are very rapid and difficult to characterize experimentally. An in-depth AIMD study of thermal decomposition process conducted Wang et al. sheds some light to these transient decomposition processes [31].

Tang et al compared the de-hydrogenation properties of ball-milled $M(BH_4)_m$– $Al(BH_4)_3(NH_3)_6$ mixtures to that of pristine $Al(BH_4)_3(NH_3)_6$ where M = Li, Na, K, Ca, Mg. The main result of this study is that with higher polarizing power of the M^{m+} cation, the decomposition temperature is lower and less ammonia impurity was released. MS study of selectively deuterated mixtures of $M(BD_4)_m$–$Al(BH_4)_3(NH_3)_6$ showed the initial release of HD gas while $M(BH_4)_m$–$Al(BD_4)_3(NH_3)$ mixture released H_2 gas. This confirmed that unlike in pristine $Al(BH_4)_3(NH_3)_6$, in the presence of $M(BH_4)_m$ its hydridic hydrogen reacted first with the protic hydrogens of ammonia molecules coordinated to aluminum cation. The polarizing power of cations in MCl_m additives also slightly decreased decomposition temperature of $Al(BH_4)_3(NH_3)_6$, however compared to $M(BH_4)_m$ additives the effect was much weaker and almost negligible [32].

Polarizing power of a cation is calculated as Z/r^2 where Z is the charge of the cation while r is the Shannon ionic radius that considers coordination number (CN) of an atom in crystalline structure [33]. Polarizing power of cations explains why KBH_4 is stable in water while $LiBH_4$ hydrolyzes and $Al(BH_4)_3$ reacts explosively. On the contrary, the polarizing power of $[Al(NH_3)_6]^{3+}$ complex cation in $Al(BH_4)_3(NH_3)_6$ roughly equals to 0.1 (the radius measured as 5.45Å from cif file of $Li_2Al(BH_4)_5(NH_3)_6$, from reference [4]). In $M(BH_4)_m$ the lower electronegativity of M means higher ionic character of the bond with borohydride group and corresponding increase of negative (Brader) charge on hydridic hydrogens of $B\text{-}H^{\delta-}$. While lower electronegativity in $[M(NH_3)_n]^{m+}$ system means lower partial positive charge on $N\text{-}H^{\delta+}$ [30]. Therefore, in $M(BH_4)_m/Al(BH_4)_3(NH_3)_6$ mixtures the dihydrogen elimination reaction is favored with increased partial charges of hydrogens in $M–B–H^{\delta-}\cdots H^{\delta'+}–N–Al$ bonds. However, this explanation does not work for AZB compounds since the coordination sphere of Zn^{2+} is not completely occupied with ammonia molecules unlike in $Al(BH_4)_3(NH_3)_6$. Zinc cation polarizes the hydrogens in both borohydride and ammonia ligands. In fact, Guo et al decreased the number of ammonia adducts in $Al(BH_4)_3(NH_3)_6$ step-wise by ball-milling it with $Al(BH_4)_3$ in various mixtures. This opened the coordination sphere of the Al^{3+} to BH_4 groups as well, resulting in distinct decrease of peak de-hydrogenation temperature from 170°C to 110°C [34].

Another study focused on the properties of similar set of materials, namely $Mg(BH_4)_2(NH_3)_2$ and $LiMg(BH_4)_3(NH_3)_2$. The main differences between these materials and AZBs are lower electronegativity of Mg^{2+} compared to Zn^{2+} (despite having similar polarizing power) and change in coordination environment of Mg^{2+} once $LiBH_4$ is incorporated into $Mg(BH_4)_2(NH_3)_2$. Similar to zinc compounds, the de-hydrogenation process takes places beyond melting temperature. But unlike $LiZn(BH_4)_3(NH_3)_2$, incorporation of $LiBH_4$ into the $Mg(BH_4)_2(NH_3)_2$ structure results in suppression of NH_3 impurity release. This is explained using DFT calculations as the ammonia vacancy formation and diffusion energy barriers being higher in bimetallic compound which prevents release of NH_3 molecules [35]. However, the energy barrier for ammonia diffusion and vacancy creation is calculated for crystalline compounds which is less relevant since decomposition of AMBs takes place in viscous melted state.

Chen et al reported a more in-depth computational analysis of $Zn(BH_4)_2(NH_3)_2$ decomposition process. The authors propose that unlike other AMBs, direct dihydrogen elimination reaction could be less likely in $Zn(BH_4)_2(NH_3)_2$. This is explained by mismatch between the calculated energy barrier for dihydrogen elimination reaction and the decomposition temperature. According to these calculations, after the melting induced amorphization process in

$Zn(BH_4)_2(NH_3)_2$, Zn^{2+} cation actively participate in H_2 release process through formation of intermediate species such as NH_3BH_3 and $[B_2H_7]^-$ by extracting a hydride H^- from $[BH_4]^-$ anions and forming Zn-H ionic bond. Furthermore, NH_3 participates in overall decomposition process through formation of $[NH_4]^+$ cation which reacts with $[BH_4]^-$ anions to release more hydrogen [18]. In our DFT calculations, to keep the model similar to bimetallic compounds a pseudo-alkali cation $A=[ZnH]^-$ is used. The presence of $A=[ZnH]^-$ represents an intermediate transient state of the decomposition process. However, $[ZnH]^-$ increases the enthalpy of "ZnN-(H2)-BZn" reaction only by 3%. Hence, this simplification does not change the conclusions of our DFT model.

5. Conclusions

A new synthesis technique based on the use of liquid ammonia as a solvent enabled direct and single step synthesis of $LiZn(BH_4)_3(NH_3)_2$, $NaZn(BH_4)_3(NH_3)_2$ and $KZn(BH_4)_3(NH_3)_2$ compounds. Among those, lithium and potassium compounds are reported for the first time in this work.

The zinc cation with two borohydride and two ammonia ligands forms the structural building block of all the reported compounds. A bimetallic $AZn(BH_4)_3(NH_3)_2$ where A = Li; Na; K on atomic level is a combination of monometallic $Zn(BH_4)_2(NH_3)_2$ and ABH_4. However, solvothermal synthesis using salt metathesis reaction inevitably results in halide anion substitution of some borohydride anions. Our ^{11}B NMR study shows that despite similar concentration of halide anion substitution, the atomic environment for $KZn(BH_4)_2Cl(NH_3)_2$ looks like $Zn(BH_4)_2(NH_3)_2$ + KCl while $KZn(BH_4)_2F(NH_3)_2$ looks more like $Zn(BH_4)F(NH_3)_2$ + KBH_4. Our DFT calculations show this difference is important enough to disable energetically favorable de-hydrogenation pathway. Regardless of the defect concentration in the structure due to the presence of alkali cations with higher polarizing power, the energetic barrier is lower for direct de-hydrogenation reaction and higher for de-ammoniation reaction resulting in better hydrogen purity.

Acknowledgement

Research activity was conducted by internal funding of CEA LITEN.

References

[1] K. Møller *et al.*, 'Complex Metal Hydrides for Hydrogen, Thermal and Electrochemical Energy Storage', *Energies*, vol. 10, no. 12, p. 1645, Oct. 2017, doi: 10.3390/en10101645.

[2] D. Teichmann, W. Arlt, P. Wasserscheid, and R. Freymann, 'A future energy supply based on Liquid Organic Hydrogen Carriers (LOHC)', *Energy Environ. Sci.*, vol. 4, no. 8, p. 2767, 2011, doi: 10.1039/c1ee01454d.

[3] M. Paskevicius *et al.*, 'Metal borohydrides and derivatives – synthesis, structure and properties', *Chem Soc Rev*, vol. 46, no. 5, pp. 1565–1634, 2017, doi: 10.1039/C6CS00705H.

[4] Y. Guo, H. Wu, W. Zhou, and X. Yu, 'Dehydrogenation Tuning of Ammine Borohydrides Using Double-Metal Cations', *J. Am. Chem. Soc.*, vol. 133, no. 13, pp. 4690–4693, Apr. 2011, doi: 10.1021/ja1105893.

[5] F. Yuan, Q. Gu, X. Chen, Y. Tan, Y. Guo, and X. Yu, 'Complex Ammine Titanium(III) Borohydrides as Advanced Solid Hydrogen-Storage Materials with Favorable Dehydrogenation Properties', *Chem. Mater.*, vol. 24, no. 17, pp. 3370–3379, Sep. 2012, doi: 10.1021/cm301387d.

[6] V. D. Makhaev, N. S. Kedrova, and N. N. Mal'tseva, 'The reaction of zinc chloride with borohydrides of the alkali metals in organic solvents', *Bull. Acad. Sci. USSR Div. Chem. Sci.*, vol. 23, no. 12, pp. 482–485, 1974.

[7] G. Xia, Q. Gu, Y. Guo, and X. Yu, 'Ammine bimetallic (Na, Zn) borohydride for advanced chemical hydrogen storage', *J. Mater. Chem.*, vol. 22, no. 15, p. 7300, 2012, doi: 10.1039/c2jm16370e.

[8] H. Nöth, E. Wiberg, and L. P. Winter, 'Boranatozinkate der Alkalimetalle', *Z. Für Anorg. Allg. Chem.*, vol. 386, pp. 73–86, 1971.

[9] G. D. Barbaras, C. Dillard, A. E. Finholt, T. Wartik, K. E. Wilzbach, and H. I. Schlesinger, 'The Preparation of the Hydrides of Zinc, Cadmium, Beryllium, Magnesium and Lithium by the Use of Lithium Aluminum Hydride', *J. Am. Chem. Soc.*, vol. 73, no. 10, pp. 4585–4590, 1951.

[10] H. Nöth, E. Wiberg, and L. P. Winter, 'Boranate und Boranato-metallate. I. Zur Kenntnis von Solvaten des Zinkboranats', *Z. Für Anorg. Allg. Chem.*, vol. 370, no. 5–6, pp. 209–223, 1969.

[11] Q. Gu *et al.*, 'Structure and decomposition of zinc borohydride ammonia adduct: towards a pure hydrogen release', *Energy Environ. Sci.*, vol. 5, no. 6, p. 7590, 2012, doi: 10.1039/c2ee02485c.

[12] D. Ravnsbaek *et al.*, 'A Series of Mixed-Metal Borohydrides', *Angew. Chem.*, vol. 121, no. 36, pp. 6787–6791, Aug. 2009, doi: 10.1002/ange.200903030.

[13] R. Černý *et al.*, 'Potassium Zinc Borohydrides Containing Triangular [Zn(BH4)3] − and Tetrahedral [Zn(BH)4xCl4–x]2– Anions', *J. Phys. Chem. C*, vol. 116, no. 1, pp. 1563–1571, Jan. 2012, doi: 10.1021/jp209848r.

[14] M. Mostajeran, D. J. Wolstenholme, C. Frazee, G. S. McGrady, and R. T. Baker, 'Solution-based routes to ammine metal borohydrides: formation of ammonia-borane', *Chem Commun*, vol. 52, no. 12, pp. 2581–2584, 2016, doi: 10.1039/C5CC10027E.

[15] P. Giannozzi *et al.*, 'QUANTUM ESPRESSO: a modular and open-source software project for quantum simulations of materials', *J. Phys. Condens. Matter*, vol. 21, no. 39, p. 395502, Sep. 2009, doi: 10.1088/0953-8984/21/39/395502.

[16] N. Varini, D. Ceresoli, L. Martin-Samos, I. Girotto, and C. Cavazzoni, 'Enhancement of DFT-calculations at petascale: Nuclear Magnetic Resonance, Hybrid Density Functional Theory and Car–Parrinello calculations', *Comput. Phys. Commun.*, vol. 184, no. 8, pp. 1827–1833, Aug. 2013, doi: 10.1016/j.cpc.2013.03.003.

[17] S. Mohan, G. Kaur, C. David, B. K. Panigrahi, and G. Amarendra, '*Ab initio* molecular dynamics simulation of threshold displacement energies and defect formation energies in $Y_4Zr_3O_{12}$', *J. Appl. Phys.*, vol. 127, no. 23, p. 235901, Jun. 2020, doi: 10.1063/5.0009543.

[18] X. Chen, W. Zou, R. Li, G. Xia, and X. Yu, 'Decomposition Mechanism of Zinc Ammine Borohydride: A First-Principles Calculation', *J. Phys. Chem. C*, Feb. 2018, doi: 10.1021/acs.jpcc.8b00455.

[19] S. Grimme, 'Semiempirical GGA-type density functional constructed with a long-range dispersion correction', *J. Comput. Chem.*, vol. 27, no. 15, 2006, doi: https://doi.org/10.1002/jcc.20495.

[20] K. Yamauchi, I. Hamada, H. Huang, and T. Oguchi, 'Role of van der Waals interaction in crystalline ammonia borane', *Appl. Phys. Lett.*, vol. 99, no. 18, p. 181904, Oct. 2011, doi: 10.1063/1.3657526.

[21] M. Abatal, A. R. Ruiz-Salvador, and N. C. Hernández, 'A DFT-based simulated annealing method for the optimization of global energy in zeolite framework systems: Application to natrolite, chabazite and clinoptilolite', *Microporous Mesoporous Mater.*, vol. 294, p. 109885, Mar. 2020, doi: 10.1016/j.micromeso.2019.109885.

[22] R. Černý, K. Chul Kim, N. Penin, V. D'Anna, H. Hagemann, and D. S. Sholl, 'AZn2(BH4)5 (A = Li, Na) and NaZn(BH4)3: Structural Studies', *J. Phys. Chem. C*, vol. 114, no. 44, pp. 19127–19133, Nov. 2010, doi: 10.1021/jp105957r.

[23] D. B. Ravnsbæk *et al.*, 'Structural studies of lithium zinc borohydride by neutron powder diffraction, Raman and NMR spectroscopy', *J. Alloys Compd.*, vol. 509, pp. S698–S704, Sep. 2011, doi: 10.1016/j.jallcom.2010.11.008.

[24] N. J. Hess *et al.*, 'Spectroscopic studies of the phase transition in ammonia borane: Raman spectroscopy of single crystal NH3BH3 as a function of temperature from 88to330K', *J. Chem. Phys.*, vol. 128, no. 3, p. 034508, Jan. 2008, doi: 10.1063/1.2820768.

[25] R. Černý *et al.*, 'NaSc(BH_4)$_4$: A Novel Scandium-Based Borohydride', *J. Phys. Chem. C*, vol. 114, no. 2, pp. 1357–1364, Jan. 2010, doi: 10.1021/jp908397w.

[26] I. Dovgaliuk, C. S. Le Duff, K. Robeyns, M. Devillers, and Y. Filinchuk, 'Mild Dehydrogenation of Ammonia Borane Complexed with Aluminum Borohydride', *Chem. Mater.*, vol. 27, no. 3, pp. 768–777, Feb. 2015, doi: 10.1021/cm503601h.

[27] S. F. Parker, 'Spectroscopy and bonding in ternary metal hydride complexes—Potential hydrogen storage media', *Coord. Chem. Rev.*, vol. 254, no. 3–4, pp. 215–234, Feb. 2010, doi: 10.1016/j.ccr.2009.06.016.

[28] Y. Yang, Y. Liu, H. Wu, W. Zhou, M. Gao, and H. Pan, 'An ammonia-stabilized mixed-cation borohydride: synthesis, structure and thermal decomposition behavior', *Phys Chem Chem Phys*, vol. 16, no. 1, pp. 135–143, 2014, doi: 10.1039/C3CP54099E.

[29] S. R. Johnson *et al.*, 'The Monoammoniate of Lithium Borohydride, Li(NH_3)BH_4: An Effective Ammonia Storage Compound', *Chem. - Asian J.*, vol. 4, no. 6, pp. 849–854, Jun. 2009, doi: 10.1002/asia.200900051.

[30] E. Welchman and T. Thonhauser, 'Decomposition mechanisms in metal borohydrides and their ammoniates', *J Mater Chem A*, vol. 5, no. 8, pp. 4084–4092, 2017, doi: 10.1039/C6TA09423F.

[31] K. Wang, Q. Liu, X.-Q. Lang, K. Tang, and J.-G. Zhang, 'What's the appropriate precondition for ammine metallic borohydrides to generate pure hydrogen?', *Int. J. Hydrog. Energy*, vol. 42, no. 22, pp. 14936–14941, Jun. 2017, doi: 10.1016/j.ijhydene.2017.05.013.

[32] Z. Tang *et al.*, 'Metal cation-promoted hydrogen generation in activated aluminium borohydride ammoniates', *Acta Mater.*, vol. 61, no. 13, pp. 4787–4796, Aug. 2013, doi: 10.1016/j.actamat.2013.05.003.

[33] M. H. Brooker and Max. A. Bredig, 'Significance of both polarizability and polarizing power of cations in nitrate vibrational spectra', *J. Chem. Phys.*, vol. 58, no. 12, pp. 5319–5321, Jun. 1973, doi: 10.1063/1.1679146.

[34] Y. Guo, Y. Jiang, G. Xia, and X. Yu, 'Ammine aluminium borohydrides: an appealing system releasing over 12 wt% pure H2 under moderate temperature', *Chem. Commun.*, vol. 48, no. 37, p. 4408, 2012, doi: 10.1039/c2cc30751k.

[35] X. Chen *et al.*, 'First-principles study of decomposition mechanisms of $Mg(BH_4)_2 \cdot 2NH_3$ and $LiMg(BH_4)_3 \cdot 2NH_3$', *RSC Adv.*, vol. 7, no. 49, pp. 31027–31032, 2017, doi: 10.1039/C7RA05322C.